Journal of Power Sources 501 (2021) 230036

Contents lists available at ScienceDirect

Journal of Power Sources

journal homepage: www.elsevier.com/locate/jpowsour

The impact of flow field plate misalignment on the gas diffusion layer intrusion and performance of a high-temperature polymer electrolyte fuel cell

Eugen Hoppe [a,b,*], Holger Janßen [a], Martin Müller [a], Werner Lehnert [a,b]

[a] Forschungszentrum Jülich GmbH, Institute of Energy and Climate Research, IEK-14: Electrochemical Process Engineering, 52425 Jülich, Germany
[b] RWTH Aachen University, Modeling in Electrochemical Process Engineering, 52062 Aachen, Germany

HIGHLIGHTS

- X-ray tomography of an inhomogeneous compressed membrane electrode assembly of a PEFC.
- Simultaneous statistical analysis of the GDL intrusion for ten channels.
- HT-PEFC single cell performance tests with flow field misalignment

GRAPHICAL ABSTRACT

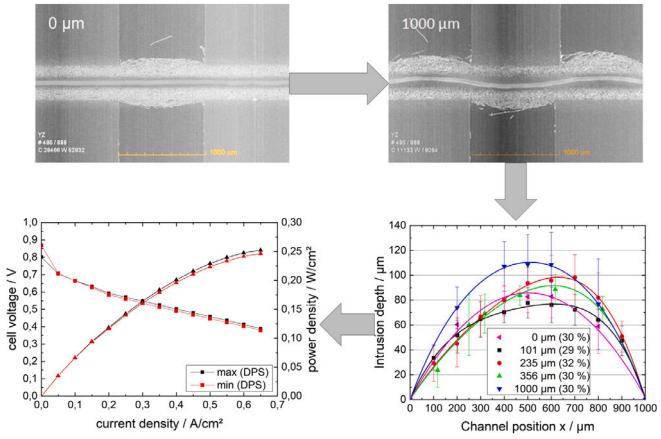

ARTICLE INFO

Keywords:
Gas diffusion layer
Membrane electrode assembly
Misalignment
Intrusion
X-ray tomography
High-temperature polymer electrolyte fuel cell

ABSTRACT

Tolerances in the production process of flow field plates for polymer electrolyte fuel cells (PEFCs) and the assembly of single cells and stacks can lead to a misalignment among the flow field plates. Due to clamping and misalignment, shear stresses can be forced on the membrane electrode assembly (MEA). Furthermore, the gas diffusion layer (GDL) intrudes into the channel. In this study, five different degrees of misalignment (0 to 1000 µm) are applied to a fuel cell model consisting of two flow field plates with five adjacent channels each (1 mm width) and an MEA in between them. For each degree, the MEA is compressed by about 30% and 3D images (tomograms) are recorded using an X-ray computer tomograph (CT). Analyzing the cross-section of the channels, the maximum intrusion depth varies for each channel. Furthermore, the shape of the membrane becomes ever more wavelike, with increasing misalignment and the position of the maximum intrusion depth shifts sideways from the center of the channel. Additionally, high-temperature polymer electrolyte fuel cell (HT-PEFC) single cell experiments are carried out. Two degrees of misalignment are set (normal assembly and 1000 µm). The performances of both degrees of misalignment are within 5% at a power density of 0.24 W.cm^{-2}.

* Corresponding author at: Forschungszentrum Jülich GmbH, Institute of Energy and Climate Research, IEK-14: Electrochemical Process Engineering, 52425 Jülich, Germany.
E-mail address: e.hoppe@fz-juelich.de (E. Hoppe).

https://doi.org/10.1016/j.jpowsour.2021.230036
Received 4 February 2021; Received in revised form 22 April 2021; Accepted 11 May 2021
Available online 18 May 2021

1. Introduction

The polymer electrolyte fuel cell (PEFC) consists of different flat components, with the membrane electrode assembly (MEA) in the middle. The reactant gas distribution across the entire active cell area, is realized by two flow field plates and two gas diffusion layers (GDL), one on the anode and one on the cathode side. To ensure gas tightness of the cell or stack and electrical and thermal conduction, the cell components must be compressed against the flow structure. Besides the gaskets, the MEA, especially the two GDLs, is the most compressed. This is due to the high porosity and low stiffness compared to the other components. The flow field plates on the anode and cathode sides often consist of sections of straight channels and ribs that face each other in the assembled cell. In most cases, it is assumed that the channels and ribs of the two flow field plates are precisely aligned. Chippar et al. [1] investigated numerically the two phase flow in a compressed GDL. Three cases were considered. In the first one, the GDL was modeled with a homogeneous porosity distribution. In the second case, different porosities were assumed under the rib and channel, and in case three the GDL intrusion was considered in addition to that of case two. To investigate the influence of different flow field designs on the performance of an high-temperature polymer electrolyte fuel cell (HT-PEFC) [2] and for predicting the contact resistance between the flow field plates and the GDL [3], in both studies the two flow field plates of the anode and cathode sides were aligned. Like Chippar et al. [1], Wu et al. [4] also modeled water transport in a single channel in a PEFC. Arlt et al. [5] and Markötter et al. [6] showed in several synchrotron measurements that there was a slight misalignment of the flow field plates. As a result of the compression and high porosity of the GDL, the GDL intrudes into the gas channel. Due to this intrusion, the gas channel is partially blocked. Based on the measurements of Arlt et al. [5] and Markötter et al. [6], the question arises as to which influence the misalignment of the flow field plates has on the GDL intrusion and the cell performance of an HT-PEFC.

Nitta et al. [7] investigated the intrusion of the GDL paper SGL10BA with a thickness of 380 µm. They used a structure of two thick aluminum plates with channel widths of 0.6 to 2 mm that were screwed together using four screws and compressed the GDL by up to 40 %. Nitta et al. [7] found that the channel width has no significant influence on the intrusion depth and reiterate the thesis that the GDL under the channel remains almost uncompressed. However, a closer look at the data indicates that with decreasing frame thickness and thus increasing compression, the GDL thickness under the channel also decreases. Tötzke et al. [8] and Haase and Rauber [9] even observed a slight increase in the thickness of a non-woven (H2315 from Freudenberg FCCT SE & Co. KG) and a non-specified GDL, respectively.

Drawing on the experimental data of Nitta et al. [7], Hottinen et al. [10] determined a function to describe the intrusion depth $h(x)$ of the paper GDL depending on the position across the channel width B:

$$h(x) = \begin{cases} h_{comp}, & x \in A \\ 19,303147 \log((x - 0,0005) \cdot 10^6 + 1) \cdot 10^{-6} + h_{comp}, & x \in B \end{cases} \quad (1)$$

h_{comp} is the compressed thickness of the GDL under the rib area A. Xu et al. [11] assume in their model the shape of the penetration to be parabolic:

$$\Delta h_{GDL} = \begin{cases} \Delta h(\frac{2x}{w})^2, & |x| \le \frac{w}{2} \\ \Delta h, & \frac{w}{2} \le |x| \le \frac{w+w_d}{2} \end{cases} \quad (2)$$

where Δh_{GDL} is the compressed thickness of the GDL at position x, Δh is the compressed thickness of the GDL under the rib, w_d is the rib width and w the channel width.

Lai et al. [12] employed a carbon paper with an uncompressed thickness of 260 µm without specifying the manufacturer. Instead of the thickness of the GDL, the contact pressure on the rib surface was controlled. In the range from 1 to 3 MPa, a linear relationship between the contact pressure and intrusion depth can be seen. For the simulation of the redistribution of the reactants to a certain number of parallel channels, Lai et al. [12] assume that the channel cross-section is decreased by the intrusion depth, and therefore that the GDL intrudes into the channel as a kind of stamp.

Saha et al. [13] investigated the pressure drop along the channel with consideration of the GDL intrusion. They carried out experimental tests, analytical calculations and computational fluid dynamics (CFD) simulations. In their analytical determination of the pressure drop, the authors proceeded equivalently to Nitta et al. [7] and Lai et al. [12] and determined the new height of the channel through the difference in the initial channel height and maximum intrusion depth of the GDL. However, from their image recordings of the compressed GDL, it can be seen that the GDL forms a parabolic intrusion shape. Saha et al. [13], like Nitta et al. [7], found that the GDL intrusion causes an increase in the pressure drop. This was also demonstrated by the experiments carried out, and enabled them to validate their simulation model. In the CFD simulations, the case in which both the intrusion behavior (shape and depth) of the GDL, as well as the change in porosity and permeability were considered, exhibited the best agreement with the experiments.

Chippar et al. [1] also investigated the influence of the GDL intrusion by means of a simulation model. In one of the three cases, as was also assumed by Lai et al. [12], Chi et al. [14] and Saha et al. [13], the GDL intrusion was modeled in the shape of a stamp, which means that the authors assume that the GDL below the channel was not compressed, as Nitta et al. [7] experimentally demonstrated. The simulations showed that the inhomogeneous compression and the intrusion of the GDL cause a significant increase in the non-uniform current density distribution across the entire MEA. However, in the simulations performed, the real shape of the intrusion was not considered. In image recordings and tomograms, a fairly parabolic intrusion form of the GDL appears independent of the type used [9,13,15–17].

In contrast to the studies shown thus far, Kandlikar et al. [18] investigated the penetration behavior in a total of eight channels with a width of 0.7 mm each for a GDL from General Motors. In a contact pressure range of 1 to 10 MPa, the intrusion depth was varied for the eight channels. For a compression pressure of 10.34 MPa the difference between the channels is even greater than for 2.07 MPa. At this pressure, the intrusion ranges from 74.2 ± 1.1 µm to 111.0 ± 1.6 µm. The authors observed that the intrusion in the outer channels was always higher than in the channels in the middle. Kandlikar et al. [18] attribute this to the fact that bracing with screws causes the flow field plate to bend and thus the GDL is pressed more strongly on the outside than on the inside. In addition to the non-optimal structure, Kandlikar et al. [18] also note the locally different compression and GDL material itself as possible reasons. In addition, Kandlikar et al. [18] as well as Lai et al. [12], showed in flow measurements along a certain number of channels that an uneven distribution of the volume flow over the channels occurs due to the different levels of GDL intrusion. Basu et al. [19] come to the same conclusion in their analytical model. These findings show the great importance of the GDL intrusion in the design of the flow field and its manifolds.

Kulkarni et al. [20] were the first to investigate the compression of an entire MEA and that between two flow field plates. For this purpose, they used a similar compression device to Tötzke et al. [8]. The examined MEA consisted of the Nafion NRE-212 membrane from Dupont, USA and the gas diffusion electrode ELE0201 was from Johnson Matthey, UK on each side. For a 1 mm channel depth and width a compression of the MEA led to a blockage of 25 % in the case of the two flow field plates and to 40 % with only one flow field plate (with a flat plate on the other side).

Liu et al. [21] simulated the pressure distribution, as well as the stress failure of the MEA for different degrees of misalignment of the bipolar plates. For the reference case, with no misalignment of the flow

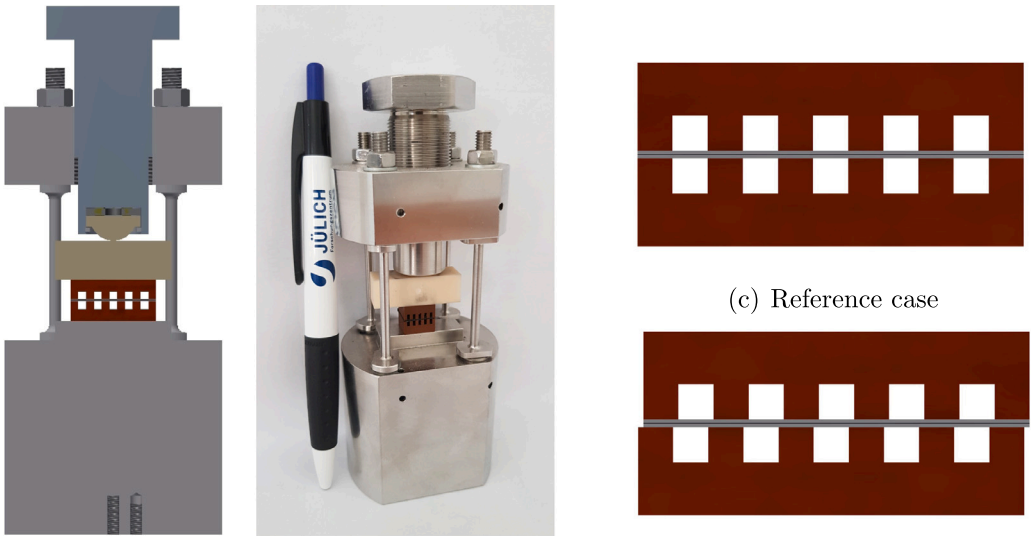

Fig. 1. (a) Experimental setup and (b) compression device. Sample stack consisting of two flow field plates with five channels each and the MEA to be investigated. (c) Without and (d) with misalignment.

field plates, they found a symmetrical and repeatable pressure distribution across the three rib widths. As the number of stacked bipolar plates and MEAs increases, the degree of misalignment decreases, from 0 ± 0.15 mm (one MEA between two bipolar plates) to 0 ± 0.111 mm (three bipolar plates) such that a certain probability of failure is maintained. Furthermore, it can be seen that there is no bending of the membrane for the reference case. With increasing misalignment the membrane bends ever more.

As far as the authors are aware, no study has yet been conducted on the intrusion behavior of the GDL for a symmetrical configuration with misalignment. Apart from that, Arlt et al. [5] and Markötter et al. [6] did not pay any further attention to the misalignment with respect to the performance of the PEFC. Therefore, in this paper the main focus is on the statistical evaluation of the GDL intrusion inside the MEA network. For this purpose, the intrusion of the GDL into ten channels is simultaneously investigated. On the one hand, the MEA is compressed by two perfectly aligned flow field plates and on the other, the MEA is compressed by misaligned flow field plates. In addition, HT-PEFC single cell tests with two different MEAs (with a woven and non-woven GDL) are carried out with. The single cells are assembled normally and with a misalignment of the flow field plates by 1000 µm. The results could then be used for modeling and flow field design purposes.

2. Materials and methods

2.1. Compression device

In order to investigate the impact of misalignment of the flow field plates of a PEFC on the MEA mechanics, a special compression device was designed. It was based on the studies of Tötzke et al. [8]. Fig. 1 shows a cut through the CAD model of the compression device and a real picture. It consists of a stainless steel frame, a screw, an axial needle bearing and a semicircular stamp. The axial needle bearing is necessary to avoid torsion of the MEA during the compression. Due to the semicircular stamp, the force is always perpendicular to the flow field plate. This also applies to the slightly inclined position of the screw. To distribute the point load across the entire flow field plate area, an additional ceramic block is placed on top of the investigated sample. In order to carry out an experiment that represents a real fuel cell, two flow field plates with an MEA in between them were used. The two flow field plates consist of five adjacent channels and six ribs with an overall size of 10 mm × 11 mm and a height of 5 mm. The average channel width of both flow field plates is approximately 0.98 mm and the average rib width is about 1.03 mm. These data were measured with the cyberSCAN CT 300 from cyberTECHNOLOGIES GmbH at a resolution of 3 µm. This corresponds approximately to the resolution of the tomograms, which is shown in chapter 2.2. For each case investigated in this study, a new MEA was used. For the MEA, the catalyst coated membrane (CCM) Gore™ Primea® from W. L. Gore & Associates GmbH and two non-woven GDLs (H2315 C2) from Freudenberg FCCT SE & Co. KG were used.

2.2. Computer tomograph

In order to carry out the experiments and analyze the compressed MEA, the computer tomograph (CT) Xradia Versa 410 from Carl Zeiss AG was used. This allows the recording of tomograms. In order to obtain the tomograms, the sample was placed on a rotating table between the source and detector. The source emits X-rays that are partially absorbed by the sample. The detector detects the incoming X-rays and transforms the information into a 2D image. During a 360° rotation, 1601 projections were taken. Of these projections, the tomogram was reconstructed. The tomograms were recorded using the parameters listed in Table 1.

2.3. Single cell

To investigate the influence of the misalignment on the cell performance of an HT-PEFC, single cells (see Fig. 2) with an active cell area of 50 cm^2 were utilized. The serpentine flow field has five parallel channels with a width and height of 1 mm. The ribs also have a width of 1 mm. In order to achieve the misalignment of the flow field plates, oblong holes were drilled in the flow field and end plate with which a misalignment of up to 1000 µm could be adjusted. Due to the compression by using screws for the assembly process of the single cell, the flow field and end plate could be fixed at the two ends of the oblong holes. Two commercially-available phosphoric acid-doped polybenzimidazole-MEAs with two different GDL types were

Table 1
Parameter CT.

Parameter	Value
Acceleration voltage	60 kV
Power	7 W
Exposure time	6 s
Distance source-sample	60 mm
Distance detector-sample	60 mm
Number of projections	1601
Rotation angle	360°
Optical magnification	4 X
Binning	2
Filter	Air
Voxel size	3.36 μm

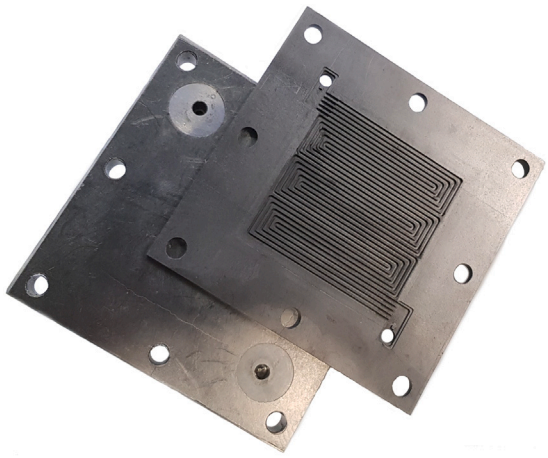

Fig. 2. Single cell with an active cell area of 50 cm^2 with a serpentine flow field and five parallel channels with a channel, rib width and height of 1 mm; the eight oblong holes enable the flow field plate's misalignment.

used. The MEA_ABM-45 MEA from Advent Technologies SA (Greece) uses a woven GDL and the Dapozol 101 Size: G77 MEA from Danish Power Systems (DPS) uses a non-woven GDL. Thus, it will also be investigated whether or not the possible influence of the misalignment is GDL-specific.

2.4. Experiments using a compression device

In order to analyze the impact of flow field plate misalignment on MEA mechanics under compression, five different cases were investigated. For the first case, the upper and lower flow field plates were aligned in such a way that the channels and ribs of both flow field plates exactly faced each other (Fig. 1(c)). Consequently, the first case serves as a reference for the others. Thus, it is possible to better assess the change in the behavior of the MEA due to the misalignment. For cases 2, 3, and 4, the misalignment was increased to 101, 235, and 356 μm, respectively (see Fig. 1(d)). The MEA was then compressed by about 30 % of its initial thickness for cases 1 to 4, as recommended by the MEA manufactures [22–24]. The compression device including the compressed sandwich consisting of the two flow field plates and the MEA is then investigated in the CT. As a fifth case, a misalignment of 1000 μm was set, which means in this case that the channels of the upper flow field plate were placed above the ribs of the lower flow field and then compressed by 30 %. The same setup was then compressed by 50 % and another tomogram measured.

2.5. GDL intrusion

For post-processing, the software TXM3DView from Carl Zeiss AG was used, which enables 2D images of the reconstructed tomogram to be generate. In contrast to the number of projections mentioned above, for each axis about 1000 2D images are generated. This is due to the number of detector pixels (max. 2048 × 2048). Depending on the binning number chosen (2), the number of pixels decreases, as 2 × 2 pixels are summarized. Each single image has a thickness of one voxel (see Table 1). As the GDL is a stochastic medium, the intrusion depth differs for each image. For a first averaging of the intrusion depth, several images are displayed at the same time. Here, 40 images are superimposed onto each other. Therefore, a certain length of the GDL is analyzed. To gain a better understanding, Fig. 3 shows a cross-section of one channel pair (3(a)) and a cut through the channel and ribs (3(b)). The area between the two dashed red lines is equivalent to the cross-section shown in Fig. 3(a). In order to determine the intrusion depth of the gas diffusion layer, the edges of the ribs were set as the zero line (the red line in Fig. 3(a)). Across the channel, five grid points at the positions of 200, 400, 500, 600, and 800 μm were chosen. The intrusion depth at each single grid point was determined by hand. Single fibers that appeared, were neglected for the analysis of the intrusion depth and shape, as the authors assumed that for a laminar flow, the single fibers would not significantly change the flow conditions of the gases along the channel. Furthermore, the intrusion shape of the fiber compound was only of interest. When discussing droplet formation, single fibers can also play an important role. To calculate the compression, the distance between the rib edges of the two flow field plates, which is equivalent to the compressed thickness of the MEA, was measured. The difference from the initial thickness was then divided by it.

2.6. CCM bending

Due to the misalignment of the flow field plates, the membrane begins to bend. In order to analyze the membrane's upward and downward shift, the straight part of the membrane serves as a reference. The degree of the shift can be used as an indicator for the magnitude of shear stresses that are applied to the membrane.

2.7. Cell tests

Following a break-in procedure, three polarization curves were measured in a row for both MEAs and assembly modes (normal and a misalignment of 1000 μm). The power density curves were calculated from the polarization curves. The polarization curves were then measured at an operating temperature of 160 °C and a stoichiometry of 2 on the anode and cathode sides. On the anode side, pure hydrogen, and on the cathode side, air, was used. Both gases were dry.

3. Results and discussion

Five different degrees of misalignment were applied to the compressed assembly, consisting of two flow field plates and an MEA. A 2D cross-section of the five channel pairs of the reference case is shown in Fig. 4(a). Comparing all ten channels of the five channel pairs, the general intrusion shape appears parabolic. Having a closer look at channel two of the upper flow field, an irregular intrusion in the right-hand section of the channel can be observed. Beyond this, the membrane remains in a flat pattern under compression and does not raise a stir. This leads to the conclusion that the applied force is mainly transmitted through the ribs.

3.1. GDL intrusion and CCM bending under flow field plate misalignment

Applying the analysis routine for the GDL intrusion, as described in the methodology section, the intrusion depth of the GDL was determined for each channel. Fig. 5 shows the intrusion of the GDL into the upper (Fig. 5(a)) and lower flow field (Fig. 5(b)) channels. Due to the stochastic nature of the GDL, the intrusion depths are

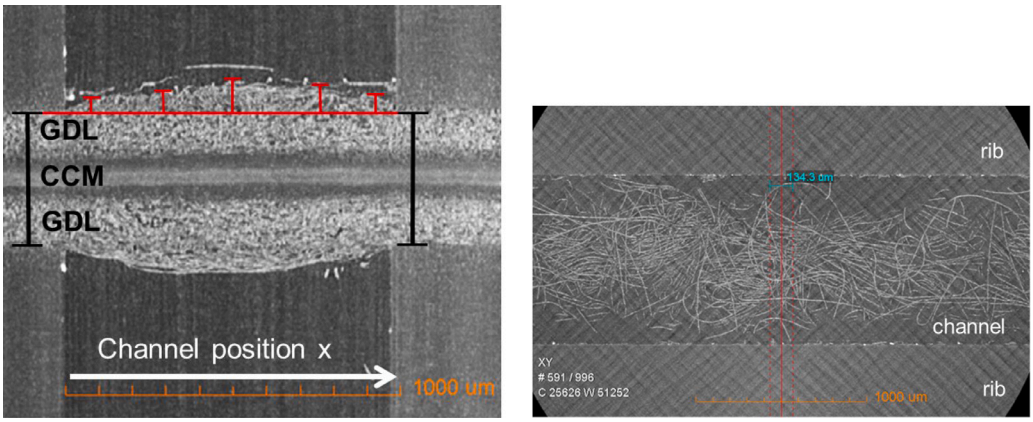

(a) Cross-section of one channel pair

(b) Cut through the top channel including the two ribs

Fig. 3. Analysis approach for the GDL intrusion. Grid points (red bars) at 0, 200, 400, 500, 600, 800 and 1000 µm. (For interpretation of the references to color in this figure legend, the reader is referred to the web version of this article.)

slightly different for the ten channels. Therefore, it is possible that the intrusion of one channel significantly differs from the other ones. This phenomenon can be observed in channel two of the upper flow field. There, the maximum intrusion depth is about 120 µm at a channel position of 600 µm. For the other channels, the maximum intrusion depth is about 90 µm. It is a coincidence that the largest as well as smallest intrusion depth occurs in channel 2. Therefore, not too much attention should be paid to this fact. Apart from the mentioned channel 2, the intrusion shape was similar for the other channels, although the GDL is a stochastic media. The channel position of the maximum intrusion depth is in the middle of the flow field channel. This can be explained by reference to the perfect alignment of the ribs, and is therefore a symmetrical compressive stress, as Kleemann et al. [25] showed in their simulations.

For a more general assertion, each grid point (0, 200, 400, 500, 600, 800, and 1000 µm) of the ten channels was averaged. The averaged intrusion depths are shown in Fig. 6 as squares. The maximum averaged intrusion depth of about 83 µm ± 17 µm is at a channel position of 600 µm and is due to the exceptional intrusion depth of channel 2 of 120 µm of the upper flow field plate. The deviation for the five grid points ranges from 12.3 µm to 21.8 µm. This underlines that the intrusion depths differ for each channel.

For simulation purposes, it may be of interest to model each individual channel with an individual intrusion depth, but it may also be of value to represent the intrusion as a function. The red curve in Fig. 6 shows the fitted curve for the measured intrusion of all ten channels. The curve was fitted with a polynomial function of the second degree. The coefficient of the determination R^2 of Eq. (4) is 0.99698. As the coefficient of the determination is high, the assumption that the intrusion shape of the GDL can be fitted as a polynomial function of the second degree is true. On the basis of the fitted function, the maximum intrusion depth is in the middle of the channel width, with an intrusion depth of about 85 µm. Concerning the initial thickness of the MEA of 560 µm, a distance between the ribs of about 390 µm and the maximum intrusion depth of 85.61 µm into both flow field channels, the MEA is not compressed at the position of the maximum intrusion depth. After transforming the equation into its vertex form, it can be seen, that the vertex is v(502.632|85.61). Taking the channel width c, the initial MEA thickness $\delta_{MEA,0}$, and the compressed thickness of the MEA δ_{MEA} into account, the vertex can be rewritten as $v(\frac{c}{2} \mid \frac{\delta_{MEA,0}-\delta_{MEA}}{2})$. Thus, for a non-woven GDL, the hypotheses can be advanced that the highest mean intrusion is dependent of the initial MEA thickness.

$$w = -\frac{3,4005 \cdot 10^{-4}}{\mu m} \cdot x^2 + 0,34184 \cdot x \Leftrightarrow \tag{3}$$

$$w = -\frac{3,4005 \cdot 10^{-4}}{\mu m} \cdot (x - 502.632\,\mu m)^2 + 85.61\,\mu m \tag{4}$$

Due to the tolerances in the fabrication process of the flow field plates and in the fuel cell assembly process, the alignment of the flow channels, especially in terms of the parallel channels on both the, anode and cathode sides, could not be perfected, as found by Arlt et al. [5] and Markötter et al. [6]. Therefore, four different degrees of misalignment were applied to the assembly used in this study. For each degree, a tomogram of every channel pair was recorded. Figs. 4(b) and 4(e) show a cross-section of the four cases. At first glance, the intrusion shape and depth appears similar for each of the four cases as well as in the reference case. In order to highlight the differences, the same diagram as that for the reference case was created. As case 1 was symmetrical for the upper and lower flow field, the position 0 was at the left-hand edge of the rib. For a proper averaging of all ten channels, the direction of the x-axis had to be inverted for the lower flow field plate. As a result, position 0 is at the right-hand edge for the lower flow field and remains the same for the upper flow field. Fig. 6 also shows also the averaged intrusion depths and fitted curves for the four cases of misalignment. For a proper fit of the curves, they were fitted with a polynomial function of the fourth degree. Each fitted function has a coefficient of determination of more than 0.99. Comparing the intrusion shape of the three cases shown in Fig. 6, the intrusion shape is no longer symmetrical, but is shifted to the right-hand side. By shifting the upper flow field plate, parts of the GDL located in the channel obtain a certain mechanical support. It can be seen that the maximum intrusion depth ranges from 70 to 100 µm. The highest intrusion depth occurs in case 2, with the highest compression rate of 32 %. In contrast, the positions of the maximum intrusion depths change with the degree of misalignment. For a misalignment of 101 and 235 µm, the position of the maximum intrusion depth is about 600 and 650 µm, respectively. For a misalignment of 356 µm, the maximum intrusion depth is around about 650 µm for the upper flow field and about 400 µm for the lower one. Taking into account that the position of maximum intrusion for the reference case is at 500 µm, and the position of maximum intrusion depth is shifted by the degree of misalignment.

Kulkarni et al. [20] showed that the porosity increases towards the surface of the GDL. As a result of the misalignment, the position of the highest porosity is also shifted, which can lead to a changed flow distribution over the channel cross-section and, consequently can influence the reactant distribution across the entire active cell area. In addition to the shift of the highest porosity, the void space between the GDL surface and channel walls changes. In a PEFC, the generated

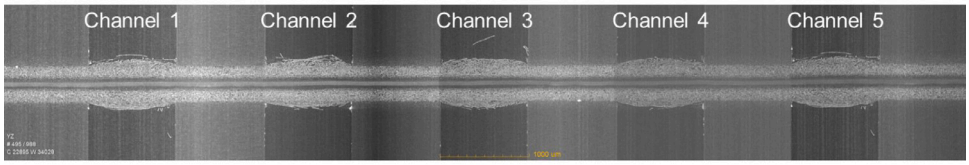

(a) 0 µm (reference case, 30 %)

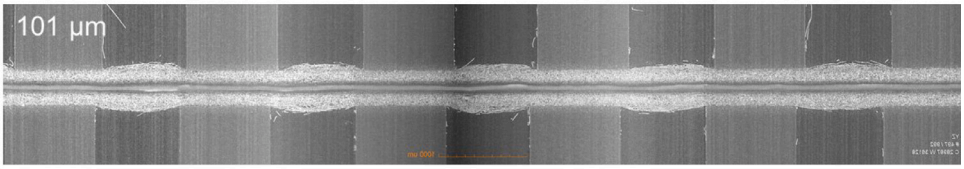

(b) 101 µm (29 %)

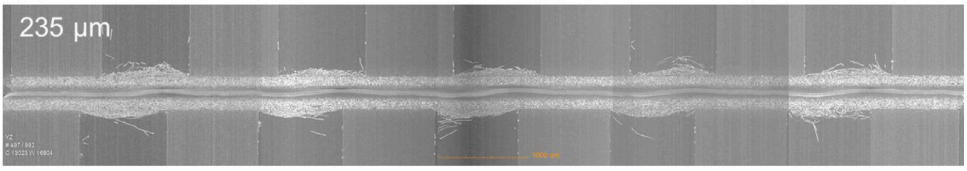

(c) 235 µm (32 %)

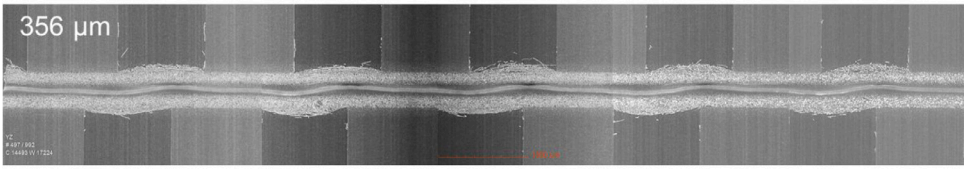

(d) 356 µm (30 %)

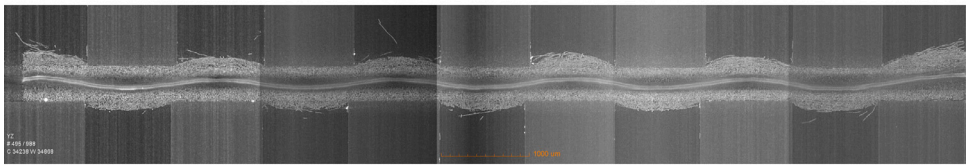

(e) 1000 µm (30 %)

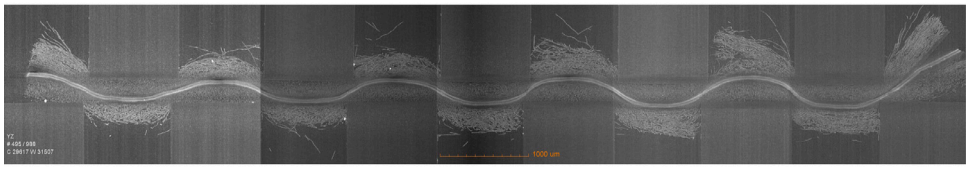

(f) 1000 µm (50 %)

Fig. 4. 2D images of the channel cross-sections for different degrees of misalignment. The actual compression is provided in the brackets.

water accumulates and forms droplets at the interface of the GDL and channel wall [6,11,26]. Therefore, the channel can be blocked on the, in our case, right side of the intruded GDL. Thus, the pressure drop over the channel would increase.

As the position of the maximum intrusion depth changes, the bending of the membrane also changes. Even with a minimum misalignment of 101 µm, an initial bending of the membrane can be identified. Increasing the misalignment leads to a higher bending of the membrane. For a shift of the flow field plates of 101 µm, the membrane is pressed up- and downwards by about 2 and 5 µm, respectively. As the voxel size is 3.36 µm, the membrane shift for case 2 is within the range of uncertainty. Increasing the misalignment to 356 µm, the membrane is pressed upwards and downwards by about 52 µm, referring to the reference case. This is a magnitude higher than the shift in case 2. Due to the bending of the membrane, it can be assumed that shear stresses have an effect on it. As a result these, the membrane may be damaged and a hydrogen cross-over can occur. Apart from the deviation shown in Fig. 6, the general behavior of both the GDL intrusion and the membrane bending repeats for each of the five channel pairs (see Fig. 4).

Fig. 4 shows the 2D views of the compressed MEA for a misalignment of 1000 µm at a compression of 30 and 50 %. It can be seen that the position of the maximum intrusion depth is again in the center of the channel. This can also be seen from the quantitative evaluation

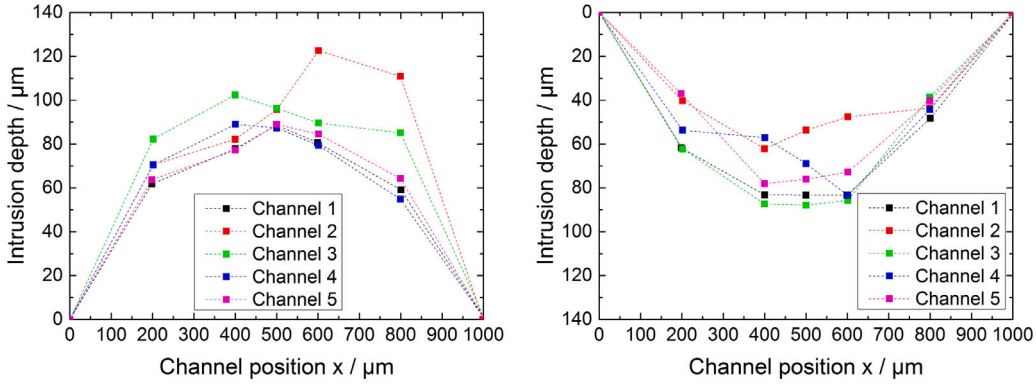

Fig. 5. Intrusion depths for the reference case for the upper and lower flow fields and the averaged and fitted intrusion depths.

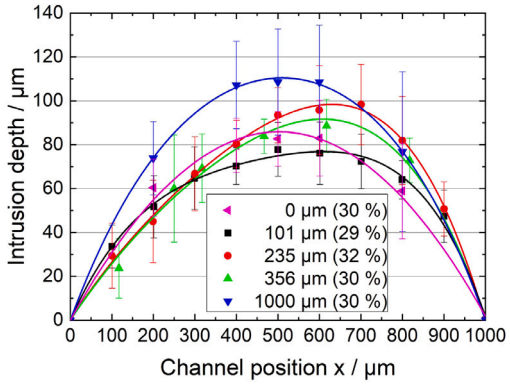

Fig. 6. Averaged (squares) and fitted (lines) intrusion depths for the five degrees of misalignment shown in Fig. 4. (For interpretation of the references to color in this figure legend, the reader is referred to the web version of this article.)

shown in Fig. 6. The averaged maximum intrusion depth for this case is about 110 µm and thus 30 % higher than in the reference case. The increase is due to the bending of the CCM in the direction of the flow channel, as the GDL is therefore also pressed more strongly into the flow channel. Increasing the compression rate from 30 to 50 % leads to a shearing of the fibers. As a result, the fibers or fiber bundles intrude into the flow channel by up to 600 µm, which leads to a massive blockage of the channel and a correspondingly major reduction in the free channel cross-section. This strongly influences the flow of the reactants. In addition, the electrical contact of the GDL to the flow field plates can also be negatively influenced, which is, consequently reflected in lower performance of the fuel cell.

If the channel width is kept constant and only the rib width is changed, this will only have a limited impact on the GDL intrusion behavior. The biggest impact would have different channel to rib ratios on anode and cathode side. In the case, where a smaller channel faces a larger one, the GDL would barely intrude into the small channel.

3.2. Performance of a single cell in presence of flow field plate misalignment

After it was shown that the misalignment of the flow field plates alters the intrusion of the GDL into the flow channel and the shape of the CCM, the influence of this on the cell's performance will be shown in the following. Before the polarization curves were measured, tomograms of one channel of the assembled test cell were taken by using the CT for the minimum and maximum misalignment. The 2D views derived from the tomograms are shown in Fig. 7. These are valid for both MEAs. It can clearly be seen that the minimum misalignment resulting from the normal assembly process is around 80 µm. In addition, the 2D views clearly show that the CCM bends even at the minimum misalignment. The black areas in the figures are artifacts of the measurements and are not considered further.

Fig. 8 shows the polarization curves for the minimum and maximum misalignment for both the Advent and DPS MEA. Three polarization curves each were measured for the four cells following a break-in procedure. In order to reach the maximum power point for each type of MEA, different current densities had to be set. The maximum power point for the Advent MEA was reached at a current density of 0.6 A cm^{-2}, whereas the maximum power point for the DPS MEA was reached at 0.7 A cm^{-2}. For the Advent MEA the setup with minimum misalignment exhibited slightly higher power densities. At a current density of 0.6 A cm^{-2}, the power density was 0.25 W cm^{-2} for the minimum displacement and 0.24 W cm^{-2} for the maximum one. Thus, the difference was only 10 mW cm^{-2}, which corresponds to a relative power density difference of 4 % with respect to the power density of the minimum misalignment.

As with the Advent MEA, the DPS MEA also indicates that the power density curves hardly differ from one another. The deviation was also found to be within the range of 5 %. Thus, for a new MEA, directly after the break-in procedure, no significant difference between the two extreme cases can be observed. If the transport and conduction paths of the gases and electrons are considered from the center of the channel or rib to the edge of it, they only minimally differ from one another. This can be clearly seen from the 2D views of the two extreme cases in Figs. 4(a) and 4(e). Apart from that, this particular single cell should be operated at a potential of about 500 mV, although it is not the maximum power point is not reached. Potentials lower than 500 mV lead (due to thermal effects) to an accelerated degradation of the cell.

4. Conclusions

As is presented in this paper, the misalignment of flow field plates has an effect on the GDL intrusion and mechanical behavior of the membrane. As the intrusion depth of the GDL into the ten channels can vary by up to 22 µm for the reference case, the free cross-section also varies. The deviation of the intrusion depth can cause a decrease in the hydraulic diameter by about 1.3 % for a 1 × 1 mm channel. For far smaller channel heights in the range of several hundred micrometers, the intrusion can have a much higher impact in terms of blocking more than half of the channel cross-section or even making contact with the channel bottom. Consequently, the pressure drop within the single channels differ. Therefore, the intrusion should be taken into account when designing the inlet and outlet manifold, as well as the

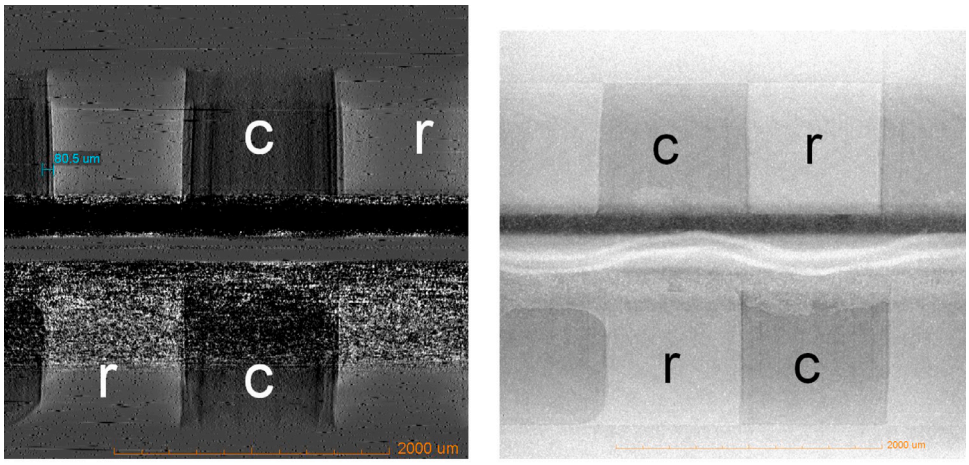

(a) Minimum misalignment (80.5 µm) (b) Maximum misalignment (1000 µm)

Fig. 7. Cross-section of the flow field plate arrangement of the assembled single cell (the degree of misalignment is valid for the Advent and DPS MEA); c: channel, r: rib.

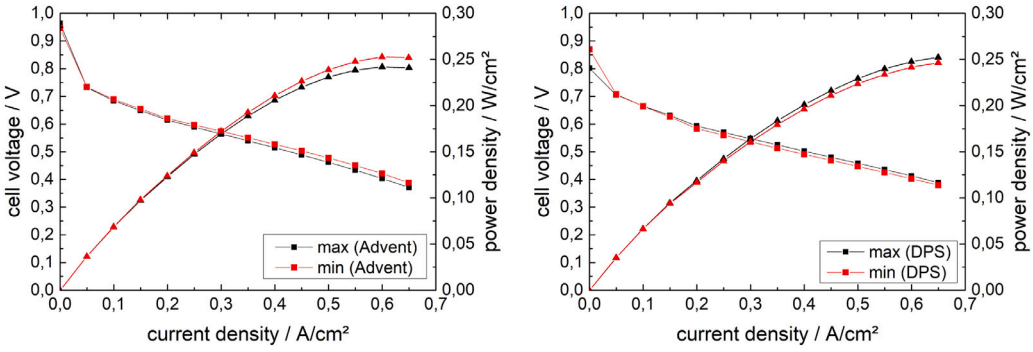

(a) MEA: Advent (b) MEA: DPS

Fig. 8. Polarization and power density curve for the single cell with two different MEAs and the two different degrees of misalignment shown in Fig. 7 at an operating temperature of 160 °C and a stoichiometry of 2 for the anode and cathode side.

channel geometry. Both manifolds should be designed to be more robust in order to avoid an inhomogeneous flow distribution. As the MEA remains uncompressed at the point of maximum intrusion, which is located at the half channel width, for the intrusion shape, a polynomial function of the second degree can be used. Furthermore, this data can be used to validate FEM-simulations of the GDL, as well as to model the GDL intrusion carrying for simulations. In practice, misalignment in the range of 100 µm are more likely to be found, as can be seen in the studies of Arlt et al. [5] and Markötter et al. [6]. Even though an extreme flow field plate misalignment by 100 % of a channel/rib width (in this case, 1000 µm) has no significant effect on the short-term cell performance of an HT-PEFC, the ex-situ investigations show that the CCM is exposed to additional shear forces, which lead to an up- and downward bending of the CCM by up to 52 µm, which can lead to membrane extension. As a result of the CCM extension, the CCM thickness can partly decrease, especially between the up- and downward bending of the CCM. This would then lead to cracks in the CCM as well as to a decrease in cell performance. In the worst case pinholes may occur and gas crossover will take place. The misalignment not only has an effect on the MEA and the GDL itself, but it can also influence the gas tightness. Depending on the sealing, misalignment can lead to an incorrect positioning of the components to ensure gas tightness. In terms of the lifetime of the single cell or stack, this could result in accelerated degradation or premature failure.

CRediT authorship contribution statement

Eugen Hoppe: Writing - original draft, Methodology, Visualization, Investigation, Conceptualization, Formal analysis. **Holger Janßen:** Supervision, Writing - review & editing, Conceptualization, Project administration, Funding acquisition. **Martin Müller:** Writing - review & editing. **Werner Lehnert:** Supervision, Writing - review & editing, Conceptualization, Project administration, Funding acquisition.

Declaration of competing interest

The authors declare that they have no known competing financial interests or personal relationships that could have appeared to influence the work reported in this paper.

Acknowledgment

The authors would like to acknowledge partial funding from the EU and North Rhine-Westphalia, Germany, grant number: EFRE-08000554.

References

[1] P. Chippar, O. Kyeongmin, K. Kang, H. Ju, A numerical investigation of the effects of GDL compression and intrusion in polymer electrolyte fuel cells (PEFCs), Int. J. Hydrogen Energy 37 (7) (2012) 6326–6338, http://dx.doi.org/10.1016/j.ijhydene.2011.04.154.

[2] T. Sousa, M. Mamlouk, K. Scott, C.M. Rangel, Three dimensional model of a high temperature PEMFC. Study of the flow field effect on performance, Fuel Cells 12 (4) (2012) 566–576, http://dx.doi.org/10.1002/fuce.201100197.
[3] Y. Zhou, G. Lin, A.J. Shih, S.J. Hu, A micro-scale model for predicting contact resistance between bipolar plate and gas diffusion layer in PEM fuel cells, J. Power Sources 163 (2) (2007) 777–783, http://dx.doi.org/10.1016/j.jpowsour.2006.09.019.
[4] H. Wu, X.G. Li, P. Berg, On the modeling of water transport in polymer electrolyte membrane fuel cells, Electrochim. Acta 54 (27) (2009) 6913–6927, http://dx.doi.org/10.1016/j.electacta.2009.06.070.
[5] T. Arlt, W. Maier, C. Tötzke, C. Wannek, H. Markötter, F. Wieder, J. Banhart, W. Lehnert, I. Manke, Synchrotron X-ray radioscopic in situ study of high-temperature polymer electrolyte fuel cells - Effect of operation conditions on structure of membrane, J. Power Sources 246 (2014) 290–298, http://dx.doi.org/10.1016/j.jpowsour.2013.07.094.
[6] H. Markötter, I. Manke, P. Krüger, T. Arlt, J. Haussmann, M. Klages, H. Riesemeier, C. Hartnig, J. Scholta, J. Banhart, Investigation of 3D water transport paths in gas diffusion layers by combined in-situ synchrotron X-ray radiography and tomography, Electrochem. Commun. 13 (9) (2011) 1001–1004, http://dx.doi.org/10.1016/j.elecom.2011.06.023.
[7] I. Nitta, T. Hottinen, O. Himanen, M. Mikkola, Inhomogeneous compression of PEMFC gas diffusion layer, J. Power Sources 171 (1) (2007) 26–36, http://dx.doi.org/10.1016/j.jpowsour.2006.11.018.
[8] C. Tötzke, G. Gaiselmann, M. Osenberg, J. Bohner, T. Arlt, H. Markötter, A. Hilger, F. Wieder, A. Kupsch, B.R. Müller, M.P. Hentschel, J. Banhart, V. Schmidt, W. Lehnert, I. Manke, Three-dimensional study of compressed gas diffusion layers using synchrotron X-ray imaging, J. Power Sources 253 (2014) 123–131, http://dx.doi.org/10.1016/j.jpowsour.2013.12.062.
[9] S. Haase, M. Rauber, Ex-situ gas diffusion layer intrusion effect determination of polymer electrolyte membrane fuel cell flow fields, J. Power Sources 291 (2015) 246–254, http://dx.doi.org/10.1016/j.jpowsour.2015.05.035.
[10] T. Hottinen, O. Himanen, S. Karvonen, I. Nitta, Inhomogeneous compression of PEMFC gas diffusion layer, J. Power Sources 171 (1) (2007) 113–121, http://dx.doi.org/10.1016/j.jpowsour.2006.10.076.
[11] Y. Xu, D. Qiu, P. Yi, S. Lan, L. Peng, An integrated model of the water transport in nonuniform compressed gas diffusion layers for PEMFC, Int. J. Hydrogen Energy 44 (26) (2019) 13777–13785, http://dx.doi.org/10.1016/j.ijhydene.2019.03.222.
[12] Y.H. Lai, P.A. Rapaport, C. Ji, V. Kumar, Channel intrusion of gas diffusion media and the effect on fuel cell performance, J. Power Sources 184 (1) (2008) 120–128, http://dx.doi.org/10.1016/j.jpowsour.2007.12.065.
[13] L.K. Saha, Y. Tabe, N. Oshima, Effect of GDL deformation on the pressure drop of polymer electrolyte fuel cell separator channel, J. Power Sources 202 (2012) 100–107, http://dx.doi.org/10.1016/j.jpowsour.2011.11.038.
[14] P.H. Chi, S.H. Chan, F.B. Weng, A. Su, P.C. Sui, N. Djilali, On the effects of non-uniform property distribution due to compression in the gas diffusion layer of a PEMFC, Int. J. Hydrogen Energy 35 (7) (2010) 2936–2948, http://dx.doi.org/10.1016/j.ijhydene.2009.05.066.
[15] J.T. Gostick, M.W. Fowler, M.D. Pritzker, M.A. Ioannidis, L.M. Behra, In-plane and through-plane gas permeability of carbon fiber electrode backing layers, J. Power Sources 162 (1) (2006) 228–238, http://dx.doi.org/10.1016/j.jpowsour.2006.06.096.
[16] I. Nitta, S. Karvonen, O. Himanen, M. Mikkola, Modelling the effect of inhomogeneous compression of GDL on local Transport Phenomena in a PEM Fuel Cell, Fuel Cells 8 (6) (2008) 410–421, http://dx.doi.org/10.1002/fuce.200700058.
[17] K.D. Baik, B.K. Hong, K. Han, M.S. Kim, Effects of anisotropic bending stiffness of gas diffusion layers on the performance of polymer electrolyte membrane fuel cells with bipolar plates employing different channel depths, Renew. Energy 69 (2014) 356–364, http://dx.doi.org/10.1016/j.renene.2014.03.060.
[18] S.G. Kandlikar, Z. Lu, T.Y. Lin, D. Cooke, M. Daino, Uneven gas diffusion layer intrusion in gas channel arrays of proton exchange membrane fuel cell and its effects on flow distribution, J. Power Sources 194 (1) (2009) 328–337, http://dx.doi.org/10.1016/j.jpowsour.2009.05.019.
[19] S. Basu, C.Y. Wang, K. Chen, Analytical model of flow maldistribution in polymer electrolyte fuel cell channels, Chem. Eng. Sci. 65 (23) (2010) 6145–6154, http://dx.doi.org/10.1016/j.ces.2010.08.036.
[20] N. Kulkarni, M.D.R. Kok, R. Jervis, F. Iacoviello, Q. Meyer, P.R. Shearing, D.J.L. Brett, The effect of non-uniform compression and flow-field arrangements on membrane electrode assemblies - X-ray computed tomography characterisation and effective parameter determination, J. Power Sources 426 (2019) 97–110, http://dx.doi.org/10.1016/j.jpowsour.2019.04.018.
[21] D.A. Liu, L.F. Peng, X.M. Lai, Effect of assembly error of bipolar plate on the contact pressure distribution and stress failure of membrane electrode assembly in proton exchange membrane fuel cell, J. Power Sources 195 (13) (2010) 4213–4221, http://dx.doi.org/10.1016/j.jpowsour.2009.12.113.
[22] Danish Power Systems Ltd., MEA manual, ver. 1.2, 2013.
[23] Danish Power Systems Ltd., Dapozol 100 MEA manual, ver. 1.4, 2014.
[24] Advent Technologies SA (Greece), Letter to Dr. Holger Janßen with attached information regarding the MEA handling, 2014.
[25] J. Kleemann, F. Finsterwalder, W. Tillmetz, Characterisation of mechanical behaviour and coupled electrical properties of polymer electrolyte membrane fuel cell gas diffusion layers, J. Power Sources 190 (1) (2009) 92–102, http://dx.doi.org/10.1016/j.jpowsour.2008.09.026.
[26] I. Manke, C. Hartnig, M. Grunerbel, W. Lehnert, N. Kardjilov, A. Haibel, A. Hilger, J. Banhart, H. Riesemeier, Investigation of water evolution and transport in fuel cells with high resolution synchrotron x-ray radiography, Appl. Phys. Lett. 90 (17) (2007) 174105, http://dx.doi.org/10.1063/1.2731440.